Relaxation of the Excited Rydberg States of Surface Electrons on Liquid Helium

Erika Kawakami,[1,2,*] Asem Elarabi,[1] and Denis Konstantinov[1,†]
[1]Quantum Dynamics Unit, Okinawa Institute of Science and Technology, Tancha 1919-1, Okinawa 904-0495, Japan
[2]PRESTO, Japan Science and Technology (JST), Kawaguchi, Saitama 332-0012, Japan

(Received 26 September 2020; accepted 28 January 2021; published 8 March 2021)

We report the first direct observation of the decay of the excited-state population in electrons trapped on the surface of liquid helium. The relaxation dynamics, which are governed by inelastic scattering processes in the system, are probed by the real-time response of the electrons to a pulsed microwave excitation. Comparison with theoretical calculations allows us to establish the dominant mechanisms of inelastic scattering for different temperatures. The longest measured relaxation time is around 1 μs at the lowest temperature of 135 mK, which is determined by the inelastic scattering due to the spontaneous two-ripplon emission process. Furthermore, the image-charge response shortly after applying microwave radiation reveals interesting population dynamics due to the multisubband structure of the system.

DOI: 10.1103/PhysRevLett.126.106802

Electrons trapped on the surface of liquid helium provide us with a unique two-dimensional electron system (2DES) [1,2]. The bound states of the electron motion perpendicular to the surface are formed due to, on one hand, the attraction of the electron to a weak image-charge inside the liquid and, on the other hand, the hard-core repulsion from the helium atoms, which prevents the electron from entering the liquid. The Rydberg states of such confined one-dimensional (1D) motion share certain similarities with the atomic spectrum of hydrogen [3–7]. At the same time, these surface electrons (SEs) can move freely parallel to the surface, which results in the subband structure of 2DES. Unlike 2DES formed in semiconductors, SEs on liquid helium are free from any crystallographic defects and impurities of the substrate. Because of the pristine nature of this system, interest in using quantum states of SEs as quantum bits has been recently growing [8–14]. In particular, spin states of SEs are expected to have longer coherence times than in any other solid-state materials [15]. Although directly accessing the spin states of SEs in an experiment is considered challenging [15], this task can be greatly facilitated by utilizing the coupling between the electron spin state and the electron motional state [12,16]. Therefore, elucidating the mechanism which governs the relaxation and dephasing of the motional states of SEs is of fundamental importance.

It has been theoretically demonstrated that the relaxation and dephasing of the electron motional states happen due to the elastic and inelastic scattering of SEs from the excitation of liquid helium [1,10,17–21]. There are two distinct liquid helium temperature ranges in this system. For high liquid helium temperatures T, the scattering is dominated by helium vapor atoms above the liquid [17,18]. For T sufficiently below 1 K, where the concentration of vapor atoms becomes small, the scattering is mostly due to the capillary waves (ripplons) excited on the surface of the liquid [18–21]. The rates of both the elastic scattering by vapor atoms and that by thermally excited ripplons decrease with decreasing T and become extremely small in the millikelvin range. Such mechanisms of elastic scattering were experimentally established by measuring the electron mobility and coincide well with the theory [17]. Contrary to that, much less is known about the inelastic ripplon scattering rate, which governs the dissipative processes in SEs at low T, such as the energy relaxation of the motional states. In terms of using the Rydberg states as qubit states, studying the mechanism of the inelastic scattering process is important because it directly affects relaxation and dephasing of the Rydberg states [10,17,19–21].

Some efforts on extracting the inelastic scattering rate from indirect measurements had been made. The intrinsic spectral linewidth of the Rydberg states should be determined by the inelastic scattering rate at sufficiently low T [7]. However, the inhomogeneous broadening of the spectral lines prevents us from extracting this rate with good precision by the conventional spectroscopic methods. In a typical experiment, due to a nonuniform electric field exerted on SEs, the inhomogeneous broadening is of the order of 1 GHz [16,22], which is about 3 orders of magnitude larger than the inelastic scattering rate, as will be shown later.

The effective electron temperature T_e should also be determined by the inelastic scattering rate via the energy-balance equation [23]. T_e can be extracted from the mobility measurement under microwave (MW) radiation [18,24]. However, it relies on a complicated relationship between the electron temperature T_e and the mobility of SEs, and thus is questionable. Although an improved method to measure T_e, which is based on the thermoelectric

(Seebeck) effect, was recently demonstrated [25], it is limited to the high-T regime.

In this Letter, we report the first direct observation of the relaxation of the Rydberg state of SEs on liquid ^{3}He in a wide range of T. This observation becomes possible thanks to the significant improvements in image-charge detection [26]. The relaxation times extracted from the decay signals show a crossover between vapor-atom and ripplon scattering regimes and reach the maximum value of about 1 μs at the lowest $T = 135$ mK used in the experiment. By comparing the measured signals and our theoretical calculations, we attribute this time to the inelastic scattering due to the spontaneous two-ripplon emission process. Moreover, we demonstrated that, at sufficiently low T, the image-charge signals become saturated shortly after applying the MW radiation due to the saturation of the population between the two lowest states. The signals eventually increase due to the subsequent leaking of the SE population to higher excited Rydberg states.

SEs are formed on the surface of liquid ^{3}He [27]. The surface of the liquid is set approximately midway between two circular electrodes of a parallel-plate capacitor with capacitance C_0. As SEs are excited from the ground ($n = 1$) state to higher ($n \geq 2$) Rydberg states, they cause a change in the image charge in the electrodes [16]. Whereas in the previous experiment the time-averaged image current was measured using a lock-in amplifier [16], in this work we measure a real-time image-charge response by employing a two-stage cryogenic broadband amplifier [26]. The first stage, which is located close to the capacitor, converts the image current into a voltage signal of which the upper bound of the bandwidth exceeds 100 MHz. The total gain of our circuit is 1. Thus both the voltage signal amplitude before amplification and the measured voltage signal can be written as $\Delta q/(C_0 + C_p)$, where $C_p \sim 10$ pF is the total parasitic capacitance of our circuit and Δq ($-\Delta q$) is the change in the image charge in the top (bottom) capacitance plate due to excitation of SEs to higher Rydberg states. As was shown previously [16], the image-charge change can be represented as

$$\Delta q = \frac{e n_s C_0}{\epsilon_0} \sum_n (\langle z \rangle_{nn} - \langle z \rangle_{11}) \rho_{nn}, \tag{1}$$

where e is the elementary charge, n_s is the density of SEs, ϵ_0 is the vacuum permittivity, $\langle z \rangle_{nn}$ is the average electron coordinate perpendicular to the surface of liquid for an electron occupying the nth Rydberg state, and ρ_{nn} is the fractional occupancy of the nth state. From the above equations, it is clear that the real-time voltage signal can capture the excited-state population dynamics in SEs, providing that the detection bandwidth is large enough compared to the excitation and relaxation rates in the system.

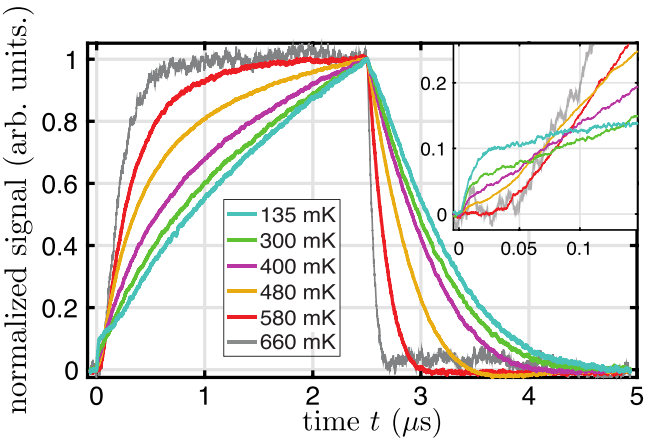

FIG. 1. Normalized voltage signals due to excitation of SEs by pulsed MW radiation at frequency $\omega/2\pi = 110$ GHz measured for different liquid helium temperatures T in the range from 135 to 660 mK. The radiation is switched on for $0 \leq t \leq 2.5$ μs and is switched off for $2.5 \leq t \leq 5$ μs. Each trace is obtained at a fixed value of T by averaging over about 10^6 repetitions. The inset shows a magnified view of the main figure in a region of t shortly after the radiation was switched on. The details of this region are discussed in the text.

In the experiment, SEs are excited by the pulse-modulated (200 kHz) MW radiation at the frequency $\omega/2\pi = 110$ GHz, which is resonant with the $n = 1 \rightarrow 2$ transition. The amplified voltage signals are averaged over approximately 10^6 repetitions using a digital storage oscilloscope. The recorded traces are corrected to eliminate the detection circuit's high-pass filtering effect [28]. Figure 1 shows an example of normalized voltage signals obtained for different T in the range from 135 to 660 mK.

First, let us investigate how the overall signals differ depending on the liquid helium temperature T. During MW excitation ($0 < t < 2.5$ μs), the voltage signals grow. At sufficiently high T, they reach a constant value, which corresponds to the steady-state population of the Rydberg states. After MW radiation is turned off at $t = 2.5$ μs, the voltage signal drops back to zero due to the relaxation of the excited-state population of SEs to the ground state.

It is well established that SEs can be strongly overheated by the resonant MW excitation, which causes a significant thermal population of the higher-lying Rydberg states [6,29]. The heating is facilitated by fast elastic scattering of the MW-excited electrons between the subbands, such that the energy absorbed by MW excitation is transferred into the energy of electron in-plane motion. Moreover, electrons redistribute energy within the same subband due to electron-electron collisions, such that SEs are described by an effective electron temperature T_e, which can significantly exceed the liquid helium temperature T [29–31]. The electron-electron collision rate is of the same order as the plasmon frequency of SE and is much higher than any rate involved here [32,33]. As a result, SEs are thermally populated to excited states, although the only transition

induced by the applied MW radiation is between the ground state and the first excited state. As the MW radiation is switched off, the decay of the excited-state population is governed by the electron energy dissipation due to inelastic scattering, upon which the energy of SEs is transferred to the liquid helium excitation.

In order to analyze the measured signals and extract the inelastic scattering rate, we performed numerical simulations and calculated the image-charge signals, taking into account the elastic and inelastic scattering processes due to both vapor atoms and ripplons. We solve the coupled time-dependent energy-balance and rate equations to find the effective electron temperature $T_e(t)$ and the fractional occupancy of the nth Rydberg state $\rho_{nn}(t)$ for the pulse-modulated MW excitation [28]. SEs are excited to the first-excited Rydberg state ($n = 2$) via electric dipole transition induced by the resonant MW field. The excitation rate r can be expressed in terms of the Rabi frequency defined as $\Omega_R = e\langle z\rangle_{12}E_{\mathrm{MW}}/\hbar$, where $e\langle z\rangle_{12}$ is the transition moment of an electron and E_{MW} is the MW amplitude, which is proportional to the square root of the incident MW power [34]. In the simulations, we assume that the excitation rate r has the Lorentzian line shape $r = 0.5\gamma\Omega_R^2/[(\Delta\omega)^2 + \gamma^2]$, where $\Delta\omega$ is the detuning from the resonance and γ is the transition linewidth. For a given temperature T, the linewidth γ is taken to be either the experimentally observed inhomogeneous linewidth or the calculated T-dependent intrinsic linewidth [17], whichever is largest. The intersubband transition rates, which enter into the rate equations for the state occupancies ρ_{nn}, are calculated by taking into account the elastic scattering due to both vapor atoms and ripplons [35]. The electron energy loss rates, which enter into the energy-balance equation, are calculated by taking into account the inelastic scattering from both vapor atoms and ripplons [35]. Following Refs. [19–21,36], we calculate the inelastic scattering rate due to ripplons by assuming a finite value of the surface potential barrier and taking the second-order term in the ripplon-induced surface displacement in the interaction Hamiltonian. By doing so, we approximate the inelastic collisions between electrons and ripplons to the two-ripplon scattering processes. Finally, the time-dependent image-charge signal for a given T is calculated as $\sum_n (\langle z\rangle_{nn} - \langle z\rangle_{11})\rho_{nn}(t)$.

Figure 2 shows the normalized image-charge signals calculated for several temperatures in the range from 135 to 580 mK and a fixed value of the Rabi frequency $\Omega_R/2\pi = 40$ MHz. As in the experiment, MW excitation is present at $0 \le t \le 2.5$ μs and is absent at $2.5 \le t \le 5$ μs. From the comparison with the normalized measured signals shown in Fig. 1, we conclude that the simulations account well for the observed behavior. It is important to emphasize that our simulations do not contain any adjustable parameters except the chosen value of the Rabi frequency Ω_R, which is determined by the applied MW power in the experiment.

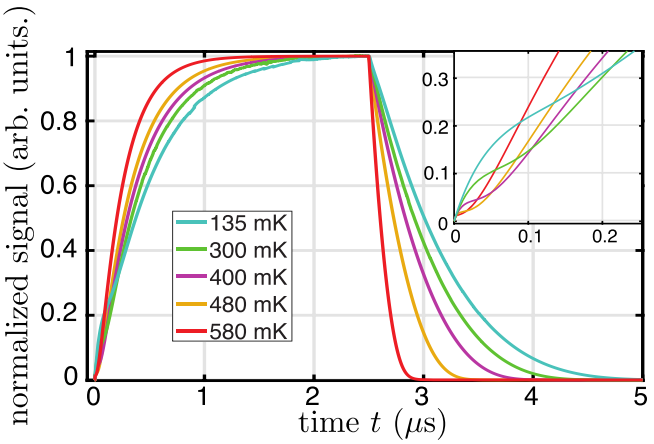

FIG. 2. (a) Semilog plot of the decaying voltage signals shown in Fig. 1 after MW is switched off. Dashed lines are fits with the exponential decay law $\exp(-t/\tau_f)$. (b) The fitting parameter τ_f (open black circles) is plotted as a function of liquid helium temperature T. The relaxation times τ_f are also extracted from the simulated decay signals (as in Fig. 3) using the same fitting procedure as in (a) and are plotted for Rabi frequency $\Omega_R/2\pi =$ 30 MHz (blue pointing down triangles), 40 MHz (purple unfilled rectangle), and 50 MHz (green pointing up triangles). The lines represent the inverse of the energy relaxation rates $\tilde{\nu}$ calculated according to Ref. [35] for $\Omega_R/2\pi = 40$ MHz (see main text), by taking into account the inelastic vapor-atom scattering (dashed line), the inelastic two-ripplon scattering (dotted line), and both processes simultaneously (solid line).

Second, let us concentrate attention on the decay signals observed after the MW radiation is turned off. Figure 2(a) shows the semilog plot of the beginning of the decaying part of the normalized measured signals shown in Fig. 1. Although the decay does not follow a simple exponential law, in order to quantify the decay rate we fit a part of the signal with the analytical expression $\exp(-t/\tau_f)$, where τ_f is a fitting parameter. The fitting curves are shown with dashed lines for each signal in Fig. 2(a). The values of τ_f extracted from the decay signals for each T are plotted in Fig. 2(b) as a function of T. As T decreases, the relaxation time τ_f rapidly increases for $400 \lesssim T \le 700$ mK. In this temperature range, the decay rate is governed by the inelastic scattering of SEs from vapor atoms, whose concentration decreases with decreasing T according to an exponential law $\exp(-Q/T)$, where Q is the latent heat of evaporation ($Q \approx 2.47$ K for ^{3}He [18]). For $135 \le T \lesssim 400$ mK, the relaxation time τ_f tends to saturate with decreasing T. The longest measured relaxation time is $\tau_f \approx 0.8$ μs at $T = 135$ mK. At low T, the concentration of vapor atoms becomes so small that the inelastic scattering is dominated by the ripplons. The conservation of momentum forbids emission of a single high-energy ripplon. According to the theory [19–21,36], the main mechanism of the electron energy loss due to the ripplons is the spontaneous generation of two short-wavelength ripplons emitted in opposite

directions. The temperature dependence of this process is much weaker than the inelastic scattering from vapor atoms.

According to Ref. [35] the electron energy loss rate $\dot{E}$ can be represented as $-(\tilde{\nu}_r + \tilde{\nu}_a)(T_e - T)$, where $\tilde{\nu}_r$ and $\tilde{\nu}_a$ are the effective energy relaxation rate for ripplon and vapor-atom scattering, respectively, which depends in a rather complicated way on the electron temperature and the state occupancies. Nevertheless, it is still instructive to compare the signal-decay rates obtained from the above fitting procedure with the rates $\tilde{\nu}_r$ and $\tilde{\nu}_a$ evaluated at a fixed value of T_e. Such numerical evaluation can be easily done by assuming thermal state occupancies according to the Boltzmanm distribution [28]. In Fig. 2(b), the inverse rates $\tilde{\nu}_r^{-1}$, $\tilde{\nu}_a^{-1}$, and $(\tilde{\nu}_r + \tilde{\nu}_a)^{-1}$ evaluated at the stationary value of T_e for SEs under MW excitation with $\Omega_R/2\pi =$ 40 MHz are plotted by the dotted, dashed, and solid lines, respectively. The temperature $T \approx 550$ mK corresponds to the crossover between the inelastic scattering regime dominated by ripplons and the one dominated by vapor atoms.

For the sake of comparison, we also plot the relaxation time τ_f extracted from the simulated decay signals for three different values of the Rabi frequency, $\Omega_R/2\pi = 30$, 40, and 50 MHz in Fig. 2(b). We found that the Rabi frequency in this range provides the best correspondence between the experimentally observed and theoretically calculated relaxation times. We note that, although the exact relationship between the applied MW power and the Rabi frequency cannot be accurately determined in the experiment, the above values of Rabi frequency are in good agreement with an earlier estimation of the Rabi frequency which was obtained from the nonlinear conductivity of SEs on liquid ^{3}He under resonant MW excitation [29].

Finally, we address an interesting behavior of the measured signals shortly after MW excitation is started; see the inset of Fig. 1. Remarkably, this rather complicated behavior is reproduced well by our numerical simulations, cf. the inset of Fig. 3. By analyzing the calculated state occupancies [28], we conclude that this behavior corresponds to the initial saturation of the first-excited state population due to MW excitation and subsequent population of the higher-excited states. At sufficiently low $T \lesssim 400$ mK, where the MW excitation rate exceeds the elastic scattering rate, the saturation of the first-excited state population causes a plateau in the measured signal. As time progresses, the elastic scattering facilitates the heating and thermal population of the higher-excited states; therefore, the signal grows toward a value corresponding to the steady-state population of many subbands. At high T, where the elastic scattering rate exceeds the excitation rate, electrons start populating the higher-excited states soon after MW excitation is started; therefore the signal steadily grows toward the stationary value. We note that this T-dependent behavior can be reproduced only for a certain range of the values of Ω_R, which define the MW excitation rate of SEs. Thus, the good agreement between the experimental data and calculations provides strong support for our estimation of the Rabi frequency in the experiment.

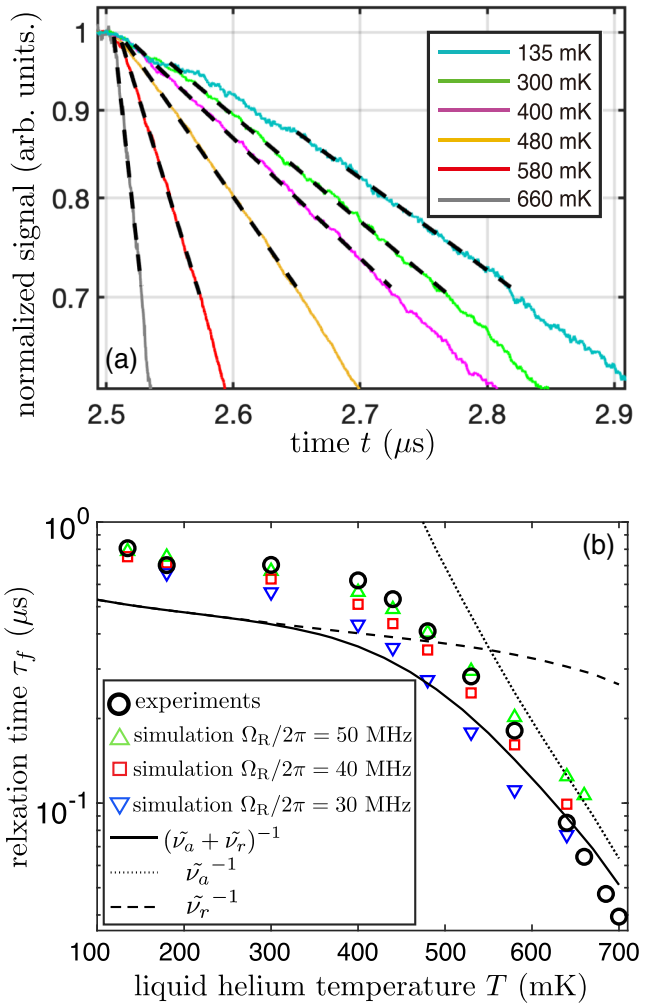

FIG. 3. Normalized image-charge signals due to excitation of SEs by pulsed MW radiation calculated using the state occupancies ρ_{nn} obtained by numerically solving the rate and energy-balance equations [28] for Rabi frequency $\Omega_R/2\pi = 40$ MHz. The inset shows a magnified view of the main figure in a region of t shortly after the excitation is started.

In summary, we described the first direct observation of the relaxation of the excited-state population in a multisubband electron system on bulk liquid helium. This allowed us to establish the temperature-dependent inelastic scattering mechanisms in the system, which will determine the quality of qubits when the Rydberg states of electrons are used as quantum bits [10]. In particular, our experimental results are well captured by the energy dissipation mechanism due to spontaneous two-ripplon emission [19–21,36]. We also demonstrated that the population of the two lowest states, the transition between which is induced by MW excitation, becomes saturated a short time

after MW radiation is started. We note that our method of fast image-charge detection can provide a valuable tool to study the two-level population dynamics in SEs. Although the elastic scattering makes higher-lying Rydberg states populated in the current experimental setup, it can be suppressed by applying a sufficiently strong (∼5 T) magnetic field perpendicular to the surface of the liquid [37]. Furthermore, our detection techniques are readily applied to electrons on thin helium film. In principle, they can also be employed in similar physical systems such as electrons on solid hydrogen and on solid neon [38].

This work was supported by JST-PRESTO (Grant No. JPMJPR1762) and an internal grant from Okinawa Institute of Science and Technology (OIST) Graduate University.

*e2006k@gmail.com
†denis@oist.jp

[1] Yu. P. Monarkha and Kono, *Two-Dimensional Coulomb Liquids and Solids* (Springer-Verlag, Berlin, 2004).
[2] *Two-Dimensional Electron Systems on Helium and Other Cryogenic Substrates*, edited by E. Y. Andrei (Kluwer Academics, Dordrecht, 1997).
[3] C. C. Grimes and T. R. Brown, Phys. Rev. Lett. **32**, 280 (1974).
[4] C. C. Grimes, T. R. Brown, M. L. Burns, and C. I. Zipfel, Phys. Rev. B **13**, 140 (1976).
[5] D. K. Lambert and P. L. Richards, Phys. Rev. Lett. **44**, 1427 (1980).
[6] A. P. Volodin and V. S. Edelman, Sov. Phys. JETP **54**, 198 (1981), http://www.jetp.ac.ru/cgi-bin/e/index/e/54/1/p198?a=list.
[7] E. Collin, W. Bailey, P. Fozooni, P. G. Frayne, P. Glasson, K. Harrabi, M. J. Lea, and G. Papageorgiou, Phys. Rev. Lett. **89**, 245301 (2002).
[8] P. M. Platzman and M. I. Dykman, Science **284**, 1967 (1999).
[9] M. J. Lea, P. G. Frayne, and Yu. Mukharsky, Fortschr. Phys. **48**, 1109 (2000).
[10] M. I. Dykman, P. M. Platzman, and P. Seddighrad, Phys. Rev. B **67**, 155402 (2003).
[11] G. Sabouret, F. R. Bradbusy, S. Shankar, J. A. Bert, and S. A. Lyon, Appl. Phys. Lett. **92**, 082104 (2008).
[12] D. I. Schuster, A. Fragner, M. I. Dykman, S. A. Lyon, and R. J. Schoelkopf, Phys. Rev. Lett. **105**, 040503 (2010).
[13] G. Yang, A. Fragner, G. Koolstra, L. Ocola, D. A. Czaplewski, R. J. Schoelkopf, and D. I. Schuster, Phys. Rev. X **6**, 011031 (2016).
[14] G. Koolstra, G. Yang, and D. I. Schuster, Nat. Commun. **10**, 5323 (2019).
[15] S. A. Lyon, Phys. Rev. A **74**, 052338 (2006).
[16] E. Kawakami, A. Elarabi, and D. Konstantinov, Phys. Rev. Lett. **123**, 086801 (2019).
[17] T. Ando, J. Phys. Soc. Jpn. **44**, 765 (1978).
[18] M. Saitoh and Aoki, J. Phys. Soc. Jpn. **44**, 71 (1978).
[19] Yu. P. Monarkha and S. S. Sokolov, Low Temp. Phys. **32**, 970 (2006).
[20] Yu. P. Monarkha and S. S. Sokolov, J. Low Temp. Phys. **148**, 157 (2007).
[21] Yu. P. Monarkha, S. S. Sokolov, A. V. Smorodin, and N. Studart, Low Temp. Phys. **36**, 565 (2010).
[22] H. Isshiki, D. Konstantinov, H. Akimoto, K. Shirahama, and K. Kono, J. Phys. Soc. Jpn. **76**, 094704 (2007).
[23] Y.-P. Monarkha, D. Konstantinov, and K. Kono, J. Phys. Soc. Jpn. **76**, 124702 (2007).
[24] A. O. Badrutdinov, D. Konstantinov, M. Watanabe, and K. Kono, Europhys. Lett. **104**, 47007 (2013).
[25] E. I. Kleinbaum and S. A. Lyon, Phys. Rev. Lett. **121**, 236801 (2018).
[26] A. Elarabi, E. Kawakami, and D. Konstantinov, J. Low Temp. Phys., (2021).
[27] ^{3}He has a significantly larger viscosity comparing with superfluid ^{4}He; therefore the electron system is less affected by the vibrations of a cryogen-free cooler used in our low-temperature setup.
[28] See Supplemental Material at http://link.aps.org/supplemental/10.1103/PhysRevLett.126.106802 for discussion of the detection circuit's high-pass filtering effect, numerical solution of coupled energy-balance and rate equations, and calculations of the stationary electron temperature and time-dependent Rydberg state occupancies.
[29] D. Konstantinov, H. Isshiki, Yu. P. Monarkha, H. Akimoto, K. Shirahama, and K. Kono, Phys. Rev. Lett. **98**. 235302 (2007).
[30] D. Konstantinov, M. I. Dykman, M. J. Lea, Y. Monarkha, and K. Kono, Phys. Rev. Lett. **103**, 096801 (2009).
[31] D. Konstantinov, M. I. Dykman, M. J. Lea, Y. P. Monarkha, and K. Kono, Phys. Rev. B **85**, 155416 (2012).
[32] D. Konstantinov, H. Isshiki, H. Akimoto, K. Shirahama, Y. Monarkha, and K. Kono, J. Phys. Soc. Jpn. **77**, 034705 (2008).
[33] R. S. Crandall, Phys. Rev. A **8**, 2136 (1973).
[34] R. Loudon, *The Quantum Theory of Light* (Oxford Science Publications, Oxford, 2000).
[35] D. Konstantinov, Y. Monarkha, and K. Kono, Fiz. Nizk. Temp. **34**, 470 (2008) [J. Low Temp. Phys. **34**, 377 (2008)].
[36] Yu. P. Monarkha, Fiz. Nizk. Temp. **4**, 1093 (1978) [Sov. J. Low Temp. Phys. **4**, 515 (1978)].
[37] A. J. Dahm, J. M. Goodkind, I. Karakurt, and S. Pilla, J. Low Temp. Phys. **126**, 709 (2002).
[38] I. I. Smolyaninov, Int. J. Mod. Phys. B **15**, 2075 (2001).